

# We are IntechOpen, the world's leading publisher of Open Access books Built by scientists, for scientists

6,900

Open access books available

186,000

International authors and editors

200M

Downloads

Our authors are among the

154

Countries delivered to

TOP 1%

most cited scientists

12.2%

Contributors from top 500 universities



WEB OF SCIENCE™

Selection of our books indexed in the Book Citation Index  
in Web of Science™ Core Collection (BKCI)

Interested in publishing with us?  
Contact [book.department@intechopen.com](mailto:book.department@intechopen.com)

Numbers displayed above are based on latest data collected.  
For more information visit [www.intechopen.com](http://www.intechopen.com)



# Towards Sustainable Rural Development in South Africa through Passive Solar Housing Design

*Ochuko K. Overen, Edson L. Meyer and Golden Makaka*

## Abstract

Rural low-cost housing in South Africa is characterised by poor thermal performance, as these houses are designed with no consideration of utilising ambient weather conditions for indoor thermal comfort. Hence, a prototype low-cost energy efficiency house was built based on the principle of passive solar design to avert the energy burden faced by low-cost house dwellers. Passive solar design in this context is the strategic selecting and locating of building envelope components to utilise the ambient weather factor of a house to enhance indoor thermal comfort. The aim of this study is to analyse the thermal performance of the passive solar house. To this effect, the indoor and weather conditions of the house which include air temperature, relative humidity, and solar radiation were monitored. The thermal contribution of the windows was determined from the measured data. In summer, 49% of the whole building air temperature and approximately 85% of its corresponding relative humidity were found within the thermal comfort. Only 23% temperature and 78% relative humidity distributions of the whole building were in the thermal comfort zone in the winter season. The daily cumulative heat contribution of the clerestory windows with no shading material was higher than that of the south-facing windows by 1.08 kWh/m<sup>2</sup>/windows in summer and 4.45 kWh/m<sup>2</sup>/windows in winter.

**Keywords:** rural development, housing, passive solar design, thermal performance, solar energy

## 1. Introduction

Over the years, building design, occupants' behaviour, choice of technology usage, and manufacturing and construction processes have resulted in the increasing energy consumption as well as the release of greenhouse gases (GHG) in the building sector [1]. Globally the building sector consumes over 30% of total final energy, having increased by more than 35% since 1990 and, at the same time, accounting for 30% of CO<sub>2</sub> gas emission. The building sector also accounts for half of the world electricity demand, with some region electricity consumption increased by 500% [2]. In the residential sector, energy is consumed for space heating, cooling, domestic activities, and lighting, among others.

However, the use of improved thermal building envelope, bioclimatic design, and energy-efficient appliance, as well as light fittings, has seen the offset of energy demand from floor and population growth in the building sector [3]. Thus, final energy demand in the building sector only rose by 5% between 2010 and 2017. Within the above specified period, a significant decline in space heating was observed, while improvement in space heating is not visible [4].

In South Africa, the housing shortage in most rural communities resulted in the mass construction of houses (low-cost) in the Reconstruction Development Program (RDP) in 1994. Since the inception of low-cost housing (LCH), more than 4.9 million households have been accommodated with over 2.3 million backlogs [5, 6]. According to Klunne, LCH are designed with no consideration of thermal energy efficiency, as they cannot utilise solar energy for space heating. He further indicated that uncontrollable heat exchange between the inner and outer space of the house due to openings and cracks on the building envelope leaves the inner space extremely cold in winter [7]. In 2005, Overy also found that the quality of LCH is poor with 90% of newly built houses not conforming to the national norms and standards. In his report, he also eluded that corruption and the use of unqualified contractors (builders) are at the forefront of the nature of the houses [8]. However, LCH dwellers tend to bear the burden as they spend a significant amount of their income to achieve thermal comfort indoors [9]. Most households that cannot afford electrical energy resort to the use of firewood, coal, paraffin heaters, or thick clothing as alternative sources of energy for heating. This results in poor indoor air quality, cold-related illness, early child motility, respiratory diseases, etc. [10, 11]. Needless to say, the provision of LCH is a positive approach to rural development in the country, but incorporating passive solar design will improve the welfare of occupants and energy consumed in space heating as well as cooling, creating sustainable rural development.

The ambient weather of a house possesses a significant amount of energy required to naturally heat or cool the inner space at little or no expense. At the same time, the uncomfortable thermal condition indoors is due to the uncontrollable interaction between the indoor and ambient weather factors [12]. Hence, to efficiently utilise the ambient weather energy indoors, a selective thermal exchange between the inner and outer environment is required; this process is known as passive solar or bioclimatic design [13]. A passive solar design uses heat movement such as conduction, convection, and radiation to admit and distribute heat in the inner space of a house.

On a typical sunny day, heat is transmitted through the windows due to radiation and conduction. The transmitted heat is stored and distributed by furniture and indoor air due to conduction and convection, respectively. Minimum infiltration air heat transfer through enhanced airtightness and controlled ventilation components are among the strategies of passive solar design. Conductive heat transfer through the perimeter walls of a passive solar house is also avoided as it is uncontrollable [14]. Regarding cooling, strategic locating and sizing of windows are used to achieve various airflow indoors. Windows at the windward and leeward side of the house create pressure difference indoors, resulting in a cross-ventilation [15, 16]. Also, locating windows or vents at significant height results in another form of airflow known as stack effect. Stack effect occurs due to vertical air temperature variation indoor. Therefore, the rate of airflow increases with an increase in the height between the upper and lower windows or vents [17].

In both aspects of passive solar design mentioned above, the windows play a vital role, considering the building envelope components, whereas the sun and wind constitute the ambient weather influencing factors. The windows in a passive solar house are strategically located and sized to take advantage of the

ambient climate condition effectively. A prototype rural LCH energy-efficient house was design and constructed in SolarWatt Park based on the principle of a passive solar house. The aim of this study is to analyse the thermal performance of the house. In the context of this study, the thermal performance of the house is analysed based on the indoor weather condition relative to the outdoor ambient weather and the windows.

## 2. SolarWatt Park and the passive solar house

SolarWatt Park is located at the University of Fort Hare, Alice, in the Eastern Cape, South Africa. Alice is classified in the temperate interior (zone 2) climate of South Africa [18]. Typical annual season of Alice is characterised by a hot summer and mild (no snow) winter, with an average dry bulb temperature of 29 and 15°C, respectively. The east wind is predominant in summer, while the winter is dominated by the west wind. An average wind speed of 2.5 m/s is experienced in Alice throughout the year [19]. A climatic map of South Africa [20], the Google earth map of SolarWatt Park and the passive solar house are presented in **Figure 1**.

The site was found suitable for the design and construction of the passive solar house due to its clear north side with no sunrays' obstacle such as tall trees, mountains and high-rise buildings. Therefore, the house was designed with its major glazing area facing north which is by the energy-efficient building design recommendation in South Africa [18, 20]. A simulated daily sun path of the house with respect to its orientation is shown in **Figure 2**.

In the northern hemisphere, north-orientated housing design guarantees optimum sunray penetration in the winter season due to the low-angle sun. The penetrated sunrays, therefore, provide heating and daylighting indoors. However, the 44-cm long eaves are used to prevent overheating indoors during the summer season by blocking direct sunrays. To this effect, the two large north-facing windows (see **Figure 2**) distribute solar radiation to the northern floor area of the house, while the clerestory windows channel solar radiance to the southern floor area. Hence, even solar radiation distribution is achieved indoors.

Meanwhile, the clerestory windows enhance indoor passive cooling due to convectional current and various wind effects through effective operations of the windows [16].

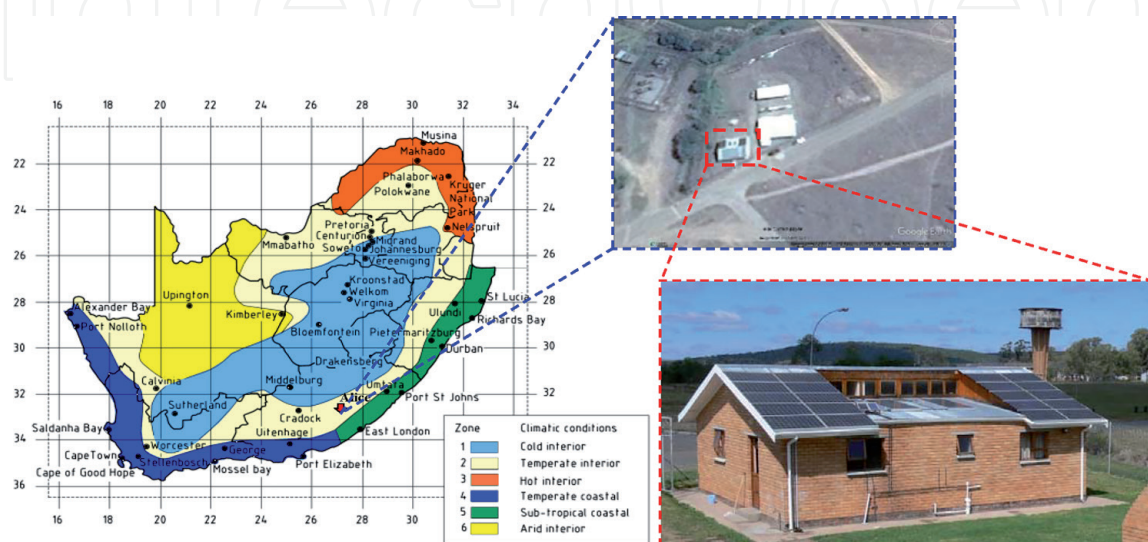


**Figure 1.** Climatic map of South Africa indicating the location of the SolarWatt Park and a photo of the passive solar house.

Furthermore, the house is made up of  $10\text{ m} \times 8\text{ m}$  ( $80\text{ m}^2$ ) floor area and consists of a bathroom, an open plan living room/kitchen and two north- and south-facing bedrooms. The floor area was arranged to ensure optimum and uniform distribution of solar radiation. The floor plan of the house indicating the floor arrangement is shown in **Figure 3**.

The floor plan was virtually partitioned into three thermal zones. Zone 1 marked with blue diagonal cross-hatch lines filled region is the living room/kitchen. The red diagonal up lines filled region used to indicate the north-facing bedroom is zone 2, while the south-facing bedroom is zone 3, represented by the region filled with green vertical lines. The bathroom was not shaded since it is not considered as a thermal zone.

In 2009, the construction of the passive solar house was estimated to be \$36,579.55 with 1.00 USD equivalent to 11.76 ZAR, while its counterpart cost is \$8505.62 [21]. In spite of the cost margin, passive solar house presents a decent home compared to conventional low-cost house [9, 16, 22].



**Figure 2.**  
A 3D view sun path simulation of the house.

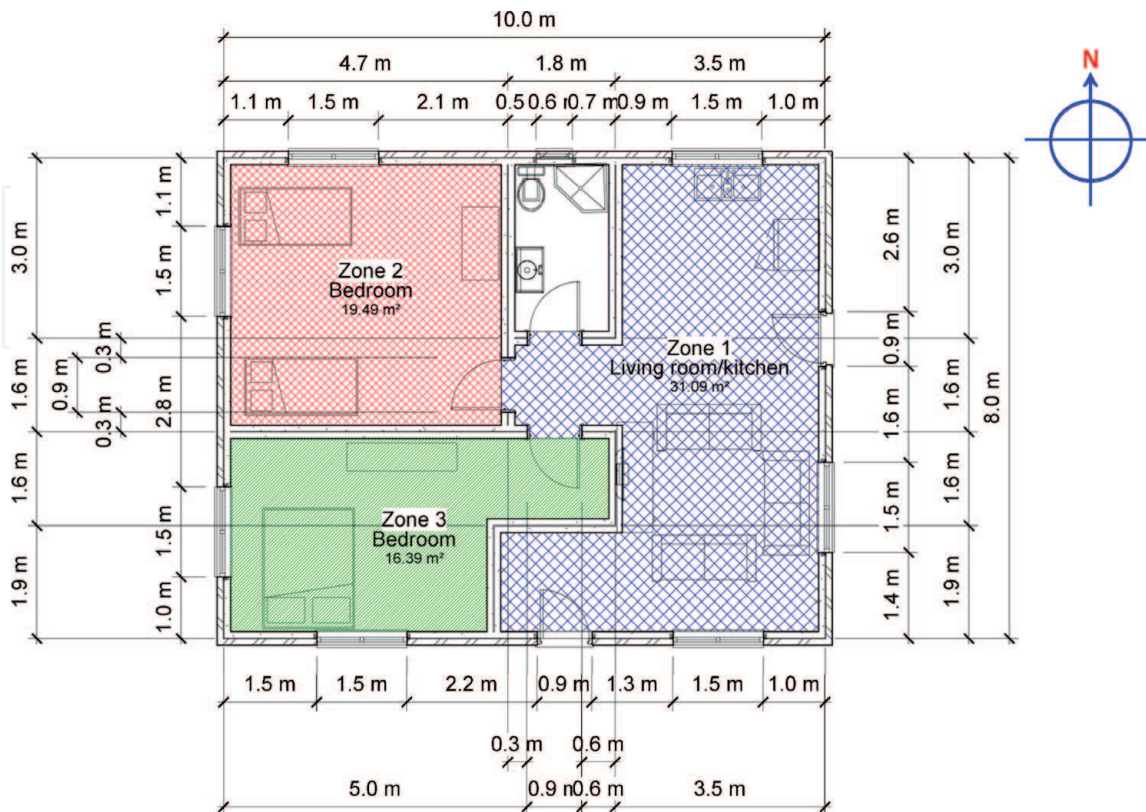


**Figure 3.**  
The floor layout of the passive solar house indicating the floor arrangement and various zone 1.

### 3. Methods and instrumentation

#### 3.1 Indoor and outdoor thermal conditions

The indoor and outdoor thermal condition measurement deals with the air temperature and relative humidity in both environments. Therefore, HMP60 temperature and relative humidity probe were used to measure the indoor as well as the outdoor air temperature and relative humidity of all zones in the house. The HMP60 probe uses a platinum resistance temperature (PRT) detector to measure air temperature, while air relative humidity is measured by capacitive relative humidity sensor [23, 24]. The measurement specifications of HMP60 probe temperature and relative humidity sensor are given in **Table 1** [25].

Three sets of HMP60 probes were used to measure the indoor air temperature and relative humidity. In each zone, one HMP60 probe was suspended at the height of 0.8 m to ensure that the measured air temperature is nearest to the temperature felt by the occupants. At the same time, the probe does not obstruct the activities of the occupants. The locations of the HMP60 probe in the house and a set outdoor weather station are indicated in **Figure 4**.

As shown in **Figure 4(b)**, the outdoor air temperature and relative humidity measuring probe was housed in a 6-plate naturally aspirated radiation shield. The white painted radiation shield enables it to reflect solar radiation. At the same time, the louvre allows natural free flow of air through the shield, thereby keeping the probe as close as possible to the ambient air temperature (eliminating solar effect) and water vapour [26].

#### 3.2 Solar radiation measurements

In this study, solar radiation measurements cover ambient global horizontal irradiance (GHI) and global irradiance at the four perimeter walls of the house. Due to atmospheric interference, the sum of direct and diffuse solar radiation reaching the earth surface, excluding albedo, is called global radiation, and it can be observed on vertical and horizontal surfaces. Thus measured global radiation on a horizontal plane is called global horizontal irradiance [27, 28].

At the right-hand side of the outdoor weather monitoring setup in **Figure 4(b)**, the horizontally levelled Kipp and Zonen CMP-11 pyranometer was used to monitor the global horizontal irradiance (GHI). The pyranometer uses a 32-junction thermopile to measure solar radiation with a sensitivity of  $8 \mu\text{V m}^{-2}$  and a spectral range of 285–2800 nm. Its response time is less than 1.7 s (63%) and 5 s (95%) [29]. The outdoor weather setup was elevated by 1 m above the roof, to ensure an unobstructed space for the radiometer. The pyranometer's dome was also cleaned twice per week to keep the dome clear of dew, dust,

Parameters	Measurement range	Accuracy ( $\pm$ )	
Temperature ( $^{\circ}\text{C}$ )	-40 to +60	0.6	
Relative humidity (%)	At 0–40 $^{\circ}\text{C}$	0–90	3
		90–100	5
	At 0–40 $^{\circ}\text{C}$ and +40 $^{\circ}\text{C}$ to +60 $^{\circ}\text{C}$	0–90	5
		90–100	7

**Table 1.**  
 HPM60 temperature and relative humidity sensor specification.

frost, birds' excreta, and any substance that may obstruct transmission of solar radiation.

Due to the daily sun movement, the solar irradiance at the elevations of a house varies. This, however, influences the thermal impact of the windows at various elevations. Thus, four Li-Cor 200R pyranometers with one pyranometer at each of the house elevation were used to monitor the global irradiance at the various elevations. **Figure 5** shows a Li-Cor 200R pyranometer measuring the global irradiance in one of the house's elevations.

As illustrated in **Figure 5**, the pyranometers were mounted vertically on the outer surface of each of the perimeter wall. They were mounted at an even height of 1.8 m. By so doing, the solar radiation falling on the walls was measured. Li-Cor pyranometer uses a silicon photovoltaic sensor mounted in a cosine-corrected head to measure solar irradiance. Together, a variable shunt resistor circuit in the cable is used to convert the measured current to a voltage signal [30].

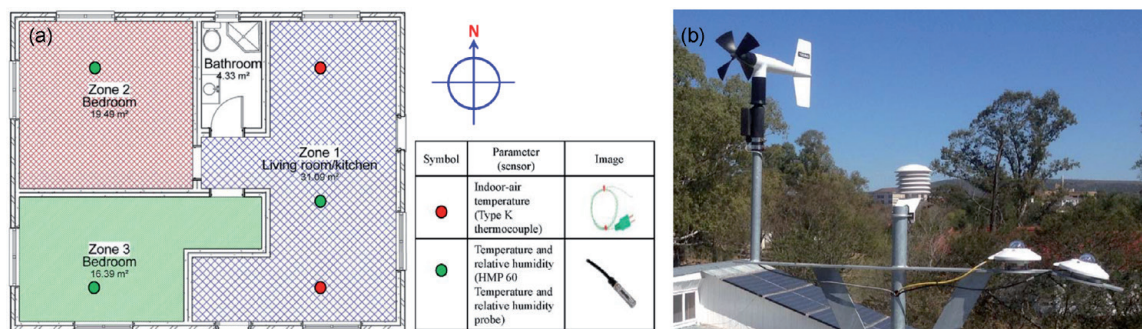


**Figure 4.**

(a) Floor layout of the house indicating the location of the indoor thermal sensor and (b) setup outdoor weather station.



**Figure 5.**

Li-Cor 200R pyranometer for monitoring global vertical irradiance on the east elevation of the passive solar house.

## 4. Results and discussions

### 4.1 Ambient solar radiation analysis

Thermal monitoring of the house which involves the global horizontal irradiance (GHI), resultant global irradiance at the various elevations, and indoor and ambient air temperature was initiated in September 2016 and continued until September 2017. Uncontrollably, 944 data entries were missed, amounting to 5% of missing data. The missing data occurs in November 2016, December 2016, February 2017, and March 2017. The periods with missing data in the affected months were excluded in the data analysis going forward.

The measured GHI and average irradiance profile are given in **Figure 6(a)**, while **Figure 6(b)** shows the monthly average GHI and total irradiation over the measurement period.

As seen in **Figure 6(a)**, due to the measurement period considered, the winter dip, represented by June, July, and August months, was obtained at the right-hand side of the profile. This, however, did not affect the measured irradiance during the entire period. In agreement with theory [31, 32], the measured GHI as seen in **Figure 4(a)** ranges from 0 to 996.0 W/m<sup>2</sup>, where periods with the sun absent produce 0 W/m<sup>2</sup> and the maximum irradiance of 996.0 W/m<sup>2</sup> was logged in February 2017 at 12 h30. Furthermore, monthly average irradiance and total irradiation were developed to portray a typical sequential distribution of annual GHI at the southern hemisphere as shown in **Figure 6(b)**. Also, the solar irradiance and irradiation distribution were predicted using a Gaussian function. The trend of the chart tends to correspond with the solar radiation distribution in the southern hemisphere [33]. In other words, a relatively lower solar irradiance of an average of 140.5 W/m<sup>2</sup> was observed in June, July, and August, whereas the rest of the months had an average of 192.8 W/m<sup>2</sup>. Due to data loss and sky formation, an irregular distribution of solar irradiance was observed in January, February, November, and December. Hence, the red and blue band areas were used to indicate the period considered as summer and winter seasons, respectively, in the thermal performance evaluation of the house.

Solar irradiance across the north, east, south, and west elevations of a house varies due to daily movement of the sun. Consequently, heat transfer through the perimeter walls varies across the elevations [34]. The global irradiance at the various elevations was measured to depict the received solar irradiance and corresponding heat transfer through the windows. Daily summer and winter average global

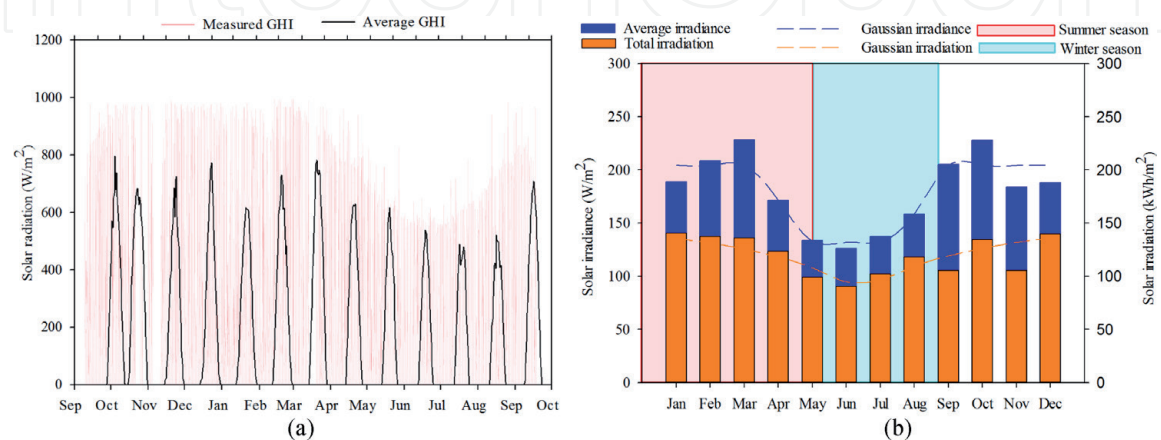


**Figure 6.**  
 (a) Measured and average global horizontal irradiance and (b) monthly average irradiance and total irradiation chart.

irradiance at the north, east, south, and west elevations, as well as their corresponding irradiation, is given in **Figure 7**.

Practically, the sun travels daily from the east to the west through the north elevation in the southern hemisphere and the south elevation in the northern hemisphere [35, 36]. The measured solar irradiance at the building elevations in **Figure 7** concurs with the above concept. Hence the north elevation receives a significant amount of solar radiation during the day, while the south elevation receives minimum daily solar radiation. Nevertheless, the solar irradiance at the north and south elevations peaked at approximately the same time (mid-day). Also, both irradiance (north and south elevations) followed the same trend as the GHI. The solar irradiance at the east and west elevations was also observed to peak at the early and late hours of the day, respectively.

The sharp dip in the west irradiance distribution was due to deciduous trees planted at the west side of the house. The trees were intended to shade the late afternoon sun and prevent cold winter wind. Further analysis of the solar radiation at the house elevations is given in **Table 2**.

As observed in **Figure 7** as well as **Table 1**, the daily average winter irradiance at the north elevation was higher than the average GHI by  $106.27 \text{ W/m}^2$ . It was also observed to be higher than the north elevation average irradiance by  $161.27 \text{ W/m}^2$  in the summer season. The relatively high north irradiance during the winter season which is due to the low-angle winter sun is the fundamental principle of passive solar design for heating concerning the ambient weather conditions. The north elevation outperformed the others regarding daily average and maximum

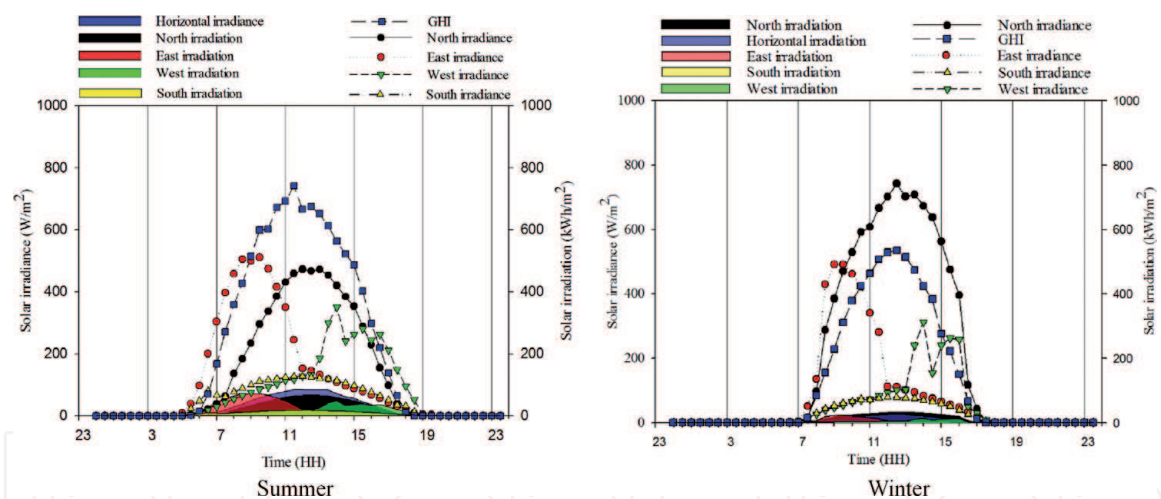


**Figure 7.** Measured solar global irradiance at the elevations of the house and corresponding heat energy on typical summer and typical winter days.

Building elevation	Summer season				Winter season			
	Average (W/m <sup>2</sup> )	Maximum (W/m <sup>2</sup> )	Peak time	Daily irradiation (kWh/m <sup>2</sup> )	Average (W/m <sup>2</sup> )	Maximum (W/m <sup>2</sup> )	Peak time	Daily irradiation (kWh/m <sup>2</sup> )
North	215.1	472.4	12 h00	3.23	376.4	741.5	12 h30	4.71
East	188.4	510.7	09 h30	2.83	156.0	490.6	9 h30	1.95
West	123.4	349.6	14 h00	1.85	92.7	311.7	14 h00	1.16
South	76.6	126.7	11 h00	1.15	44.2	78.0	12 h00	0.55

**Table 2.** Typical summer day solar global radiation at the house elevations.

irradiance as well as the daily irradiation, comparing other elevations in **Table 1**. The solar irradiation in **Figure 7(a)** and **(b)** serves as the instantaneous (30 min interval) heat energy received from the sun at the respective elevation, whereas, **Table 1** gives the daily cumulative heat energy. Per day, the north elevation had the maximum heat energy during the winter season.

#### 4.2 Windows heat transfer and solar heat gain

Heat transfer through the windows of a house is the sum of conductive and radiative heat transfer. During the day (present of the sun), both means of heat transfer coincide. While at night, conductive heat transfer is dominant. Due to the indoor and ambient air temperature difference, conductive heat transfer transpires through the windows. Conductive heat transfer through the windows is given as [37]

$$Q_{c\theta} = \sum AU(T_{eo} - T_i) \quad (1)$$

where  $A$  is the area of the window including the frame,  $U$  is the conductive heat transfer coefficient, and  $T_i$  represents indoor air temperature. The ambient air temperature was replaced by  $T_{eo}$  in Eq. (1). As indicated in **Table 1**, the daily irradiance varies across the house elevations; it is, however, not viable to quantify the conductive heat transfer through each window, assuming a uniform ambient air temperature. Thus, a parameter that incorporates the ambient air temperature and solar radiation was introduced to evaluate the heat transfer through the windows; this parameter is called as sol-air temperature  $T_{eo}$ . Sol-air temperature also caters for convective and radiative heat transfer between the windows and ambient air film. Sol-air temperature is given by [38]:

$$T_{eo} = T_o + \frac{\alpha I}{h_o} - \frac{\Delta q_{ir}}{h_o} \quad (2)$$

$h_o$  represents the surface (convective and radiative) heat transfer coefficient ( $\text{W/m}^2 \text{K}$ ), while  $I$  is global solar irradiance at a given elevation ( $\text{W/m}^2$ ).  $\Delta q_{ir}$  is the correction to infrared radiation transfer between a surface and the environment, if the sky temperature is different from  $T_o$  ( $\text{W/m}^2$ ). Furthermore,  $\alpha$  is the absorptance of the surface for solar radiation. Using Eq. (2) and **Figure 7**, the average summer and winter sol-air temperature at the various elevations of the passive solar house was computed and given in **Figure 8**.

In computing the sol-air temperature, longwave radiation factor ( $\frac{\Delta q_{ir}}{h_o}$ ) was assumed to be  $0^\circ\text{C}$  for the windows, considering that they are vertically inclined to the sunrays. Regarding solar absorption  $\alpha$  of the surfaces, a dark-coloured surface of  $0.053 \text{ m}^2 \text{ K/W}$  was assumed [36], since the perimeter walls and the wooden frame of the windows were dark in colour. Comparing **Figures 9** and **7**, the sol-air temperature at each of the house elevation corresponds to their respective global irradiance. Both parameters (sol-air temperature and global irradiance) were observed to follow the same trend and peaks at the same time. However, during the absence of the sun, the sol-air temperature at the various elevations of the house was found to be approximately equal.

The sun is solely responsible for radiative heat transfer. Hence, radiative heat transfer only occurs during the period the sun is present, and it is referred to as solar heat gain. Equation (1) must be positive to achieve solar heat gain. However, the instantaneous radiative or solar heat gain through a window can be evaluated by

$$Q_{sol} = A \times SC \times SHGF \quad (3)$$

where  $SC$  is the shading coefficient of the window. It varies with respect to the type of glazing and shading device (blind, drape, etc.). Depending on the reflection, absorption, and transmission of the glazing and shading device, a significant amount of solar heat gain is reduced or transferred through the window. An inverse function of the  $SC$  is the solar heat gain factor ( $SHGF$ ).  $SHGF$  is the fraction of solar heat transmitted through a specific window. Hence,  $SHGF$  takes into consideration the geographical location of the window; time of the day, month, and year; as well as orientation of the window. The  $SHGF$  for windows in specific locations on the earth with respect to the parameters as mentioned above is given by ASHRAE [38]. However, a universal substitute for  $SHGF$  is the solar heat gain coefficient ( $SHGC$ ). The relationship between both parameters are given as

$$SHGF = SHGC \times I \quad (4)$$

Therefore Eq. (3) can be rewritten as

$$Q_{sol} = A \times SC \times SHGC \times I \quad (5)$$

Hence, the instantaneous heat transfer through the house windows at the various elevations was computed by combining Eqs. (1) and (5) together with **Figures 7 and 8**. The resultant summer and winter daily heat transfer through the house windows is given in **Figure 9(a) and (b)**, respectively.

The following assumptions were made to obtain the profile given in **Figure 10**. The  $SHGC$  and  $U$ -value of a timber frame window are 0.77 and  $5.6 \text{ W/m}^2 \text{ K}$ , respectively [18]. In all windows excluding the clerestory windows, semiopen weave and medium colour single drapes were used. Hence, the  $SC$  of the windows was 0.51. On the other hand, no drapes were used in the clerestory windows; thus the  $SC$  was 0.95 [39]. The area of the frame and thermal lag factor of the windows were ignored. In terms of operation, all windows were closed at all times.

In both figures, the north-facing windows had the maximum heat gain. This includes the clerestory and north perimeter windows. Heat gain through the clerestory windows was found to be maximum with 759 W at 14 h00 and 1356.50 W at 12 h30, in summer and winter, respectively. The daily average heat gain through the same windows was 507.72 W in summer and 896.51 W in winter. The north

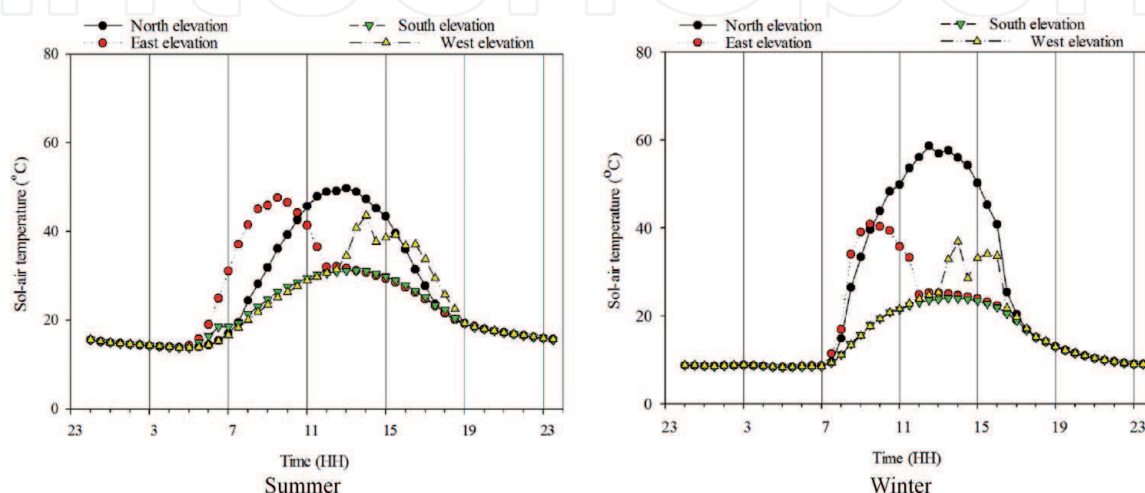


**Figure 8.** Sol-air temperature at various elevations of a passive solar house on average summer and winter days.

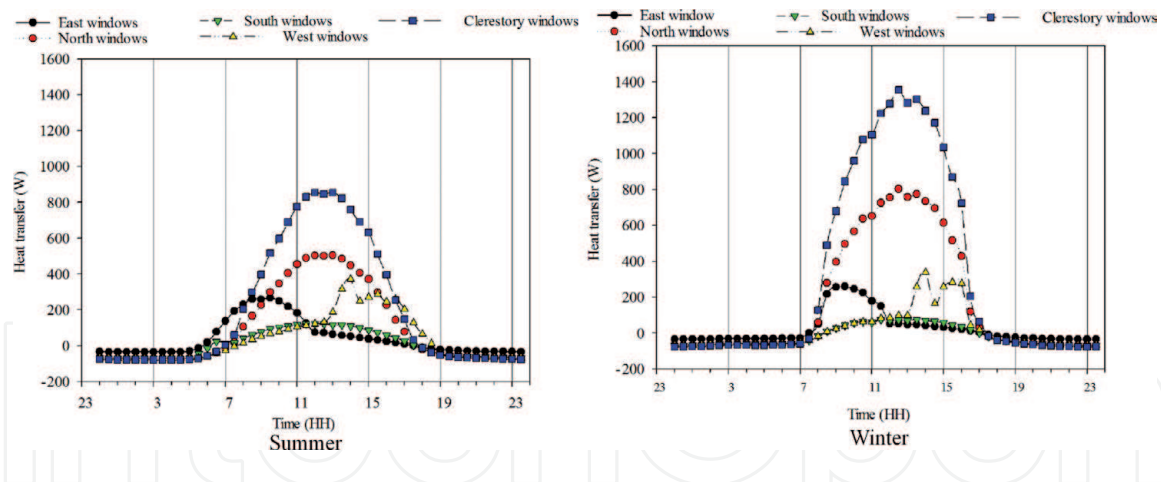


**Figure 9.** Typical summer and winter daily heat transfer through the windows of a passive solar house.

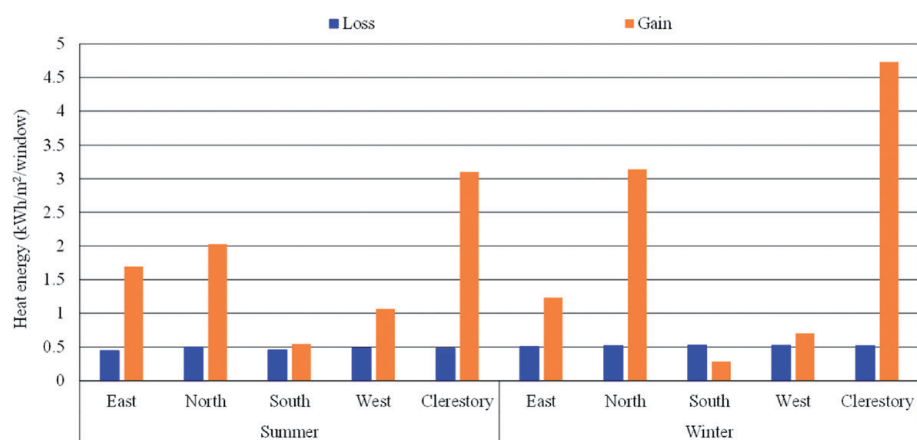


**Figure 10.** Seasonal daily windows' cumulative heat energy.

perimeter windows' heat transfer follows the same trend but 79 and 41% lesser in summer and winter, respectively.

The least heat gain was obtained at the south perimeter windows. Their daily average heat gain was 76.29 W in summer and 50.85 W in winter. Heat transfer through the south windows was 85% lesser than that of the clerestory windows in summer and 94% lower in the winter season. The clerestory windows also had the maximum heat loss. The daily average heat loss difference between the clerestory windows and the other perimeter windows was 15.62 and 14.42 W in summer and winter, respectively. Furthermore, the daily cumulative heat energy through the windows in summer and winter is given in **Figure 10**.

The clerestory windows generate 3.10 kWh/m<sup>2</sup>/window in summer and 4.73 kWh/m<sup>2</sup>/window in winter. This results in 9.30 and 18.60 kWh/m<sup>2</sup> daily cumulative heat energy generated in the living room and south-facing bedroom in summer, as well as 14.19 kWh/m<sup>2</sup> in the living room and 28.38 kWh/m<sup>2</sup> in the south-facing bedroom in winter. Once again, the south perimeter windows were the most under-performing. The daily cumulative heat energy gain through the south windows was 82 and 94% lesser than that of the clerestory windows in summer and winter, respectively. An average daily cumulative heat energy loss of 0.48 kWh/m<sup>2</sup>/window was obtained in all windows in summer. Also in winter, 0.52 kWh/m<sup>2</sup>/window was obtained. Besides, the east perimeter windows had the maximum heat energy loss with 0.45 kWh/m<sup>2</sup>/window in summer and 0.51 kWh/m<sup>2</sup>/window in winter.

The clerestory windows show significant heat contribution to the inner space of the house. From the findings, it indicates that the clerestory windows were able to

offset the underperforming south perimeter windows. Also, irrespective of size (glass surface area), the clerestory windows outperformed the other windows in both seasons in terms of heat gain. It can be said that the performance of the windows is a factor of the orientation of the house rather than the surface area of the windows (glass). Additionally, the solar heat gain through the windows was examined. The summer and winter daily average solar irradiation on the outer surface of the house windows and the resultant heat energy gain are given in **Figures 11** and **12**, respectively.

From **Figure 11**, the south perimeter windows had minimum heat energy transmission. It was found that 48%/window of solar irradiation was transmitted through the south perimeter windows. The clerestory windows, on the other hand, had the maximum heat energy transmission with 96%/window. Similar behaviour was observed in **Figure 12**. The south perimeter and clerestory windows heat energy transmission with respect to their solar irradiation were 52 and 101%/window, respectively. Detailed findings of the solar irradiation of the house windows and the resultant heat energy transmission are given in **Table 3**.

As stated earlier, the heat energy transmitted through the windows (glass area) is due to simultaneous conductive and radiative heat transfer. Although, the above comparative analysis only took into consideration the radiative heat energy generated on the windows' outer surface. Also, no shading device (drapes) was used in the clerestory windows. Hence, during the winter season, more than 100% of heat energy was transmitted through the clerestory windows.

### 4.3 Indoor weather conditions analysis

The indoor air temperature and relative humidity were the focus of the indoor weather conditions analysis. Thus, both parameters of each zone in the house were measured separately to establish the thermal influence of the various activities and orientation of the rooms (see **Figure 4**). The seasonal daily indoor air temperature and relative humidity profiles of the different zones in the house are given in **Figure 13**.

In **Figure 13**, the vertical bar charts below and above represent the air temperature and relative humidity percentage difference, respectively, of the three zones. A minimal summer day air temperature and relative humidity percentage difference were observed. However, zone 3 had the maximum air temperature and relative

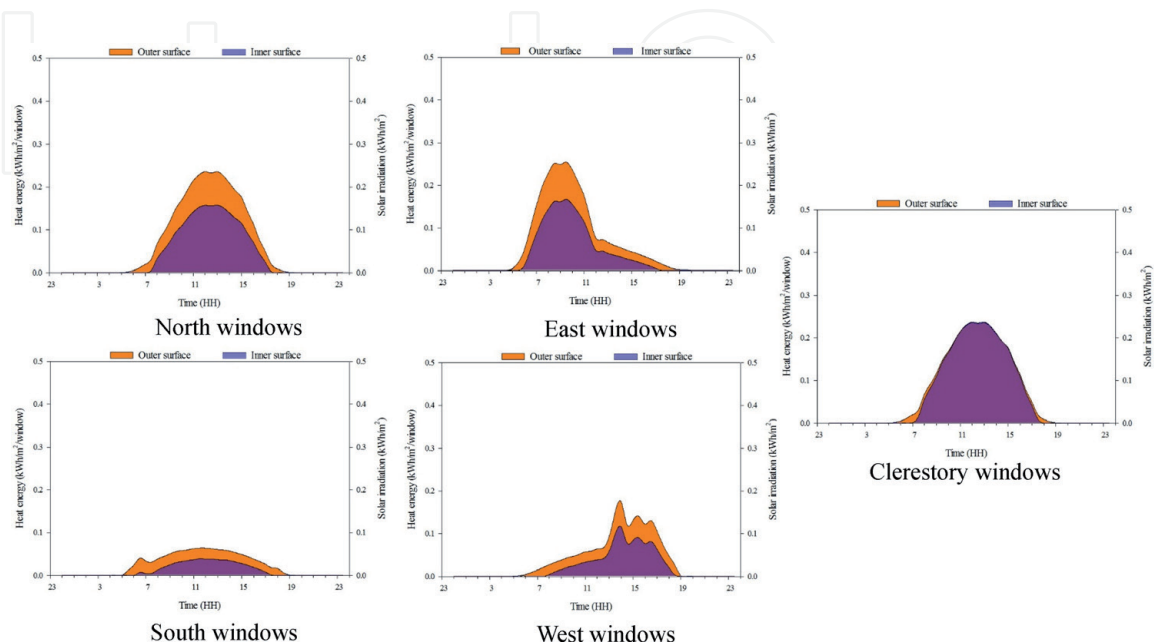


**Figure 11.** Typical summer day solar heat gain of the house north, east, south, west, and clerestory windows.

humidity percentage difference in both days. On a typical summer day, the air temperature percentage difference was 4% at 12 h00 and a corresponding relative humidity of 3% at 11 h00. The air temperature and relative humidity percentage differences were, respectively, 16% and 12% on a typical winter day. Further findings of **Figure 13** are summarised in **Table 4**.

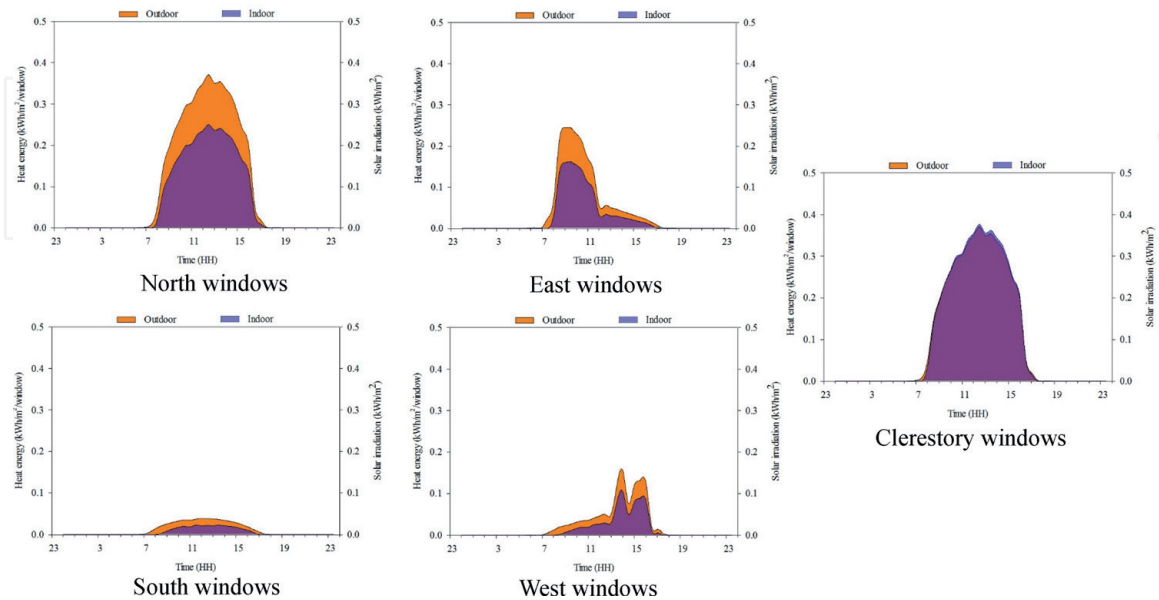


**Figure 12.**  
 Typical winter day solar heat gain of the house north, east, south, west, and clerestory windows.

Windows	Summer		Winter	
	Solar irradiation (kWh/m <sup>2</sup> )	Transmitted heat energy (%/window)	Solar irradiation (kWh/m <sup>2</sup> )	Transmitted heat energy (%/window)
North	3.23	63	4.71	67
East	2.83	60	1.95	63
South	1.15	48	0.55	52
West	1.85	57	1.16	61
Clerestory	3.23	96	4.71	101

**Table 3.**  
 Seasonal solar heat energy transmitted through the windows.

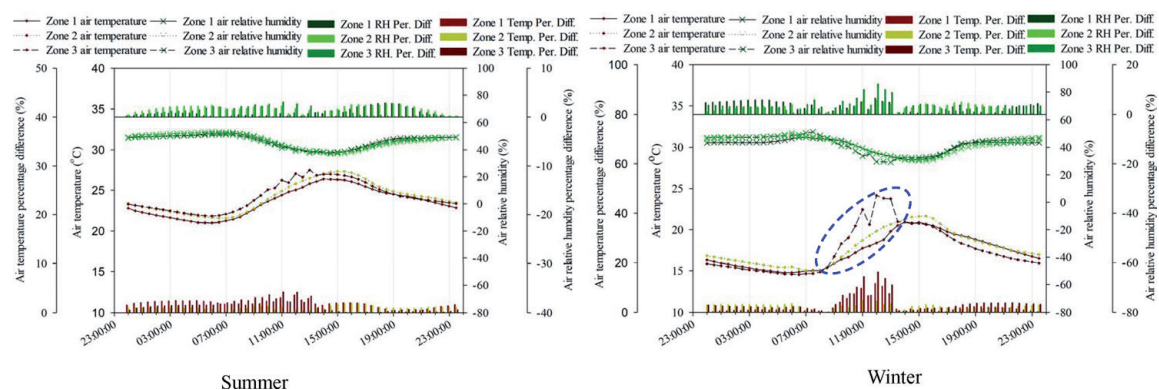


**Figure 13.**  
 Average summer and winter days' air temperature and relative humidity distribution in the various zone.

In **Tables 4** and **5**, the daily swing refers to the difference between the daily maximum and minimum air temperature and relative humidity. In **Table 4**, a fairly constant daily air temperature swing with an average of 5.6°C was observed, although the relative humidity swing in each zone varies. This was expected given that the presence and activities of occupants in a room are an influencing factor of relative humidity.

Furthermore, varying air temperature and relative humidity were observed in each zone during the typical winter day. This implies that a relatively high diurnal temperature variation was experienced during the winter season. In addition, zone 3 had the maximum daily air temperature swing of 9.6°C. This was as a result of the north-facing clerestory windows. Recall that the house was designed to optimise even air temperature indoors. Hence, the clerestory windows were installed to distribute solar radiation to the south floor area of the house. The blue dash circles in **Figure 13** indicate air temperature increase in zone 3 (south-facing room) due to penetrated solar radiation, consequently increasing the day and night air temperature differences in the zone. Zone 3 air temperature tends to increase more in winter due to the low-angled sun experienced during the season, regarding the blue circled area in both figures.

However, the average indoor air temperature and relative humidity in all zones were obtained and used to illustrate the indoor air temperature and relative humidity distribution within the thermal comfort zone. The average air temperature of all zones was represented by the whole building air temperature, while whole building relative humidity served as the average relative humidity of the three zones. Summer season frequency distribution of the whole building and ambient air temperature, as well as their corresponding relative humidity, are shown in **Figure 14**.

Zone	1		2		3	
Indoor weather parameter	Temp. (°C)	RH (%)	Temp. (°C)	RH (%)	Temp. (°C)	RH (%)
Daily swing	5.4	14.4	5.8	16.1	5.7	13.5
Max. per. diff. (%) (equiv. temp.)	4 (0.9°C)	2.9 (1.3%)	2 (0.5°C)	2.7 (1.2%)	4 (1.1°C)	3.1 (1.3%)
Peak time	12 h00	18 h30	16 h00	18 h30	11 h00	11 h00
Average per. diff. (%) (equiv. temp.)	2 (0.4°C)	0.9 (0.4%)	1 (0.2°C)	1.7 (0.8%)	1 (0.3°C)	1.1 (0.5%)

**Table 4.** Typical summer day indoor air temperature and relative humidity variation in the house zones.

Zone	1		2		3	
Indoor weather parameter	Temp. (°C)	RH (%)	Temp. (°C)	RH (%)	Temp. (°C)	RH (%)
Daily swing	6.1	16.3	6.7	20.0	9.6	22.2
Max. per. diff. (%) (equiv. temp.)	11.6 (2.4°C)	6.5 (2.2%)	4.8 (0.9°C)	5.7 (1.9%)	16.2 (3.4°C)	12.2 (4.1%)
Peak time	12 h00	12 h00	11 h00	12 h00	12 h00	12 h00
Average per. diff. (%) (equiv. temp.)	2.2 (0.4°C)	3.1 (1.3%)	2.3 (0.4°C)	2.5 (1.0%)	3.9 (0.7°C)	3.6 (1.5%)

**Table 5.** Typical winter day indoor air temperature and relative humidity variation in the house zones.

A total of 12,607 data entries were used to develop the summer whole building and ambient air temperature and relative humidity distribution profile. As seen in **Figure 14**, the whole building and ambient air temperature distributions were divided into nine classes of 4.9°C width, and the air relative humidity frequency distribution curve is made of 11 classes of 9.99% width. Statistically, the whole building and ambient air temperature were not normally distributed. The whole building temperature skewness was 0.20 with a standard error (S.E) of 0.02, whereas a skewness of 0.41 (S.E 0.02) was obtained for the ambient temperature. Although both whole building and ambient air relative humidity in **Figure 14** were also not normally distributed, an opposite skewness was obtained. The whole building and ambient relative humidity had a skewness of  $-23.32$  and  $-23.68$ , respectively, both with a S.E of 0.02.

This implies that the measured air temperature and relative humidity deviate away from their mean towards the positive and negative side, respectively, where the whole building and ambient mean values are indicated by the blue broken (24°C) and solid (19°C) lines in their respective classes. The broken red line (47%) is used to identify the mean value of the whole building relative humidity, while the solid red line signifies the mean ambient relative humidity of 68%.

Thermally in **Figure 14**, the solid grey line and band indicate the indoor air temperature (20 and 24°C) and relative humidity (30 and 60%) comfort zones, respectively [40]. In this regard, 49% of the whole building air temperature and approximately 85% of its corresponding relative humidity were found within the thermal comfort, whereas only 21 and 28% of the ambient air temperature and relative humidity, respectively, were in the thermal comfort zone.

In the winter season, a total of 4386 data entries were used to develop the whole building thermal condition, ambient air temperature, and relative humidity distribution profile. Nonetheless, a similar behaviour of the whole building, ambient air temperature, and relative humidity were observed. **Figure 15** shows the measured ambient and whole building air temperature as well as the resultant relative humidity during the winter season.

From **Figure 15**, the whole building temperature and relative humidity skewness were 0.22 and  $-0.21$ , respectively, with a S.E of 0.04. Meanwhile, a skewness of 0.22 was observed for the ambient air temperature, while the relative humidity skewness was  $-0.15$ , both with a S.E of 0.04. Hence, the whole building, ambient air temperature, and relative humidity curves are asymmetric. In other words, the mean of the whole building air temperature drifts away from the thermal comfort zone, leaving only 23% of the whole building temperature distribution in the

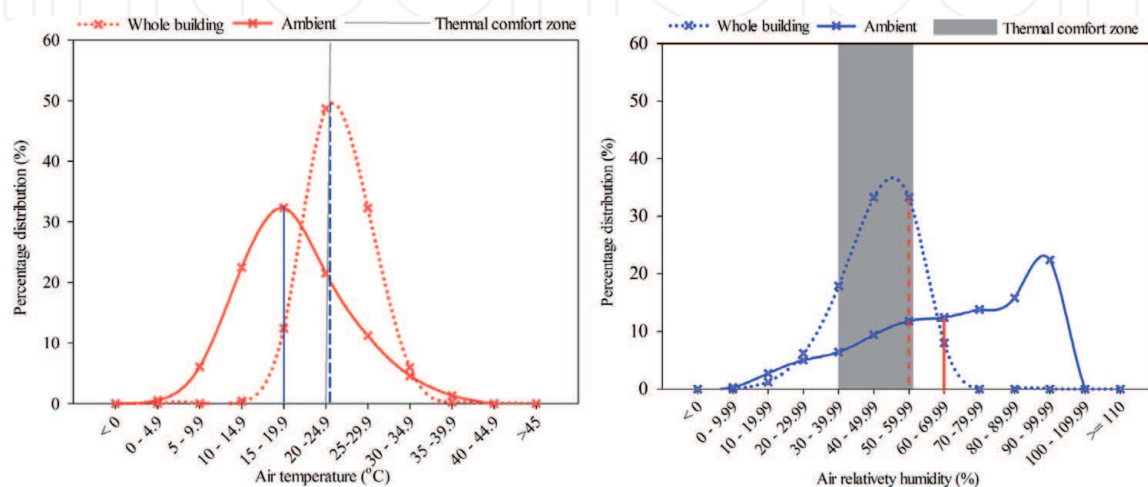


**Figure 14.** Whole building and ambient air temperature and relative humidity summer season profile.

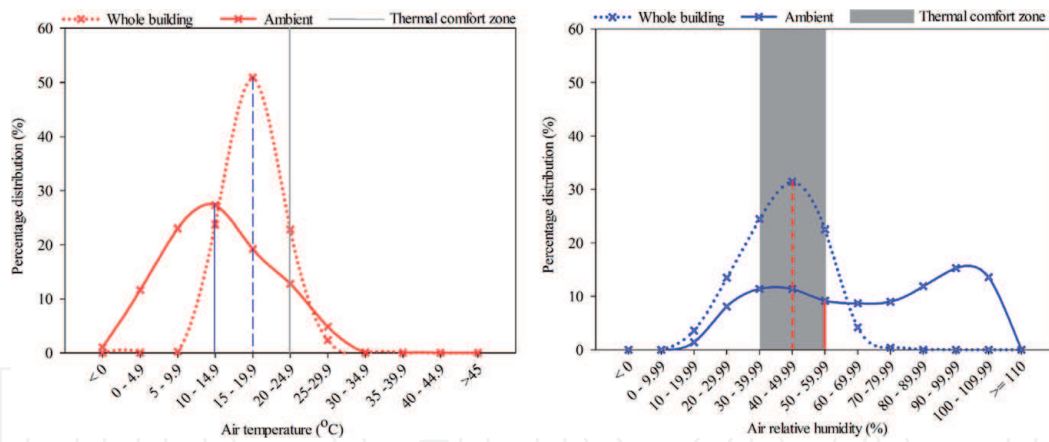


**Figure 15.** Whole building and ambient air temperature and relative humidity winter season profile.

thermal comfort zone. However, the percentage of the ambient air temperature in the thermal comfort zone deviates by 10%, whereas approximately 78 and 29% of the whole building and ambient air relative humidity, respectively, were inside the thermal comfort zone.

Based on the findings, it could be said that the whole building air temperature to a certain degree is influenced by the ambient air temperature given that both distributions follow the same trend in both seasons. Nevertheless, the same cannot be said for the whole building and ambient air relative humidity. In both seasons, the whole building relative humidity distribution tends to follow the whole building air temperature.

Theoretically, relative humidity is a measure in percentage of the amount of water vapour in the air compared to the amount of water vapour the air can hold at a given temperature. Considering that the amount of water vapour the air can hold mainly depends on the air temperature, an increase in air temperature increases the capacity of water vapour the air can hold. At a fixed amount of water vapour, an increase in air temperature results in a decrease of the air relative humidity and vice versa. Therefore, the measured air temperature and relative humidity in **Figures 14** and **15** are in line with theory.

## 5. Conclusion

The aim of this study is to analyse the thermal performance of a prototype low-cost energy-efficient house in South Africa. A passive solar house in SolarWatt Park, Alice, was used in the study. The indoor and ambient weather conditions of the house were monitored. Indoor and outdoor air temperature, relative humidity, as well as global horizontal irradiance and global irradiance at the various elevations of the house constitute the weather conditions.

It was found that strategic locating of the windows provides significant daylighting and heating for the inner space of the house. Also, the heat contribution of the windows was found to be dependent on the house orientation and shading materials (blind and drape). The performance of the north-facing clerestory and south-facing windows supports this claim. The daily cumulative heat contribution of the clerestory windows with no shading material was higher than that of the south-facing windows by 1.08 kWh/m<sup>2</sup>/windows in summer and 4.45 kWh/m<sup>2</sup>/windows in winter. Due to conductive and radiative heat transfer which co-occurs in the windows, the clerestory windows were found to transmit more than 100% of the solar radiative energy generated on the outer surface in winter. The performance

of the clerestory windows as shown in the findings made it an essential component of direct solar heat gain strategy in passive solar design.

It was also observed that the generated heat from the windows does not constitute overheating indoor. In summer, 49% of the whole building air temperature and approximately 85% of its corresponding relative humidity were found within the thermal comfort. Only 23% temperature and 78% relative humidity distributions of the whole building were in the thermal comfort zone in the winter season.

## Acknowledgements

This work was based on the research supported in part by the National Research Foundation of South Africa (Grant number 116763). We also acknowledge the Department of Science and Technology and Govan Mbeki Research and Development Centre for supporting this research.

## Conflict of interest

The authors declared no conflicts of interest regarding the authorship of this publication.

## Author details

Ochuko K. Overen\*, Edson L. Meyer and Golden Makaka  
University of Fort Hare, Fort Hare Institute of Technology, Alice, South Africa

\*Address all correspondence to: [ooveren@ufh.ac.za](mailto:ooveren@ufh.ac.za)

## IntechOpen

© 2019 The Author(s). Licensee IntechOpen. This chapter is distributed under the terms of the Creative Commons Attribution License (<http://creativecommons.org/licenses/by/3.0>), which permits unrestricted use, distribution, and reproduction in any medium, provided the original work is properly cited. 

## References

- [1] Blok K, Geng L, Harvey D, Lang S, Levermore G, Mehlwana M, et al. Residential and commercial buildings. In: *Clim. Chang. 2007 Work. Gr. III Mitig. Clim. Chang.* New York: Cambridge; 2007. pp. 387-446
- [2] International Energy Agency. *Energy Technology Perspectives 2016: Towards Sustainable Urban Energy Systems.* Paris: International Energy Agency; 2016
- [3] International Energy Agency and the United Nations Environment Programme. *2018 Global Status Report: Towards a zero-emission, efficient and resilient buildings and construction sector.* Germany: United Nation Environment; 2018
- [4] IEA. *Energy Efficiency 2018—Analysis and outlooks to 2040.* Paris: International Energy Agency; 2018
- [5] Msindo BYE. *Housing backlog Protests and the demand for Housing in South Africa.* Johannesburg: Public Service Accountability Monitor; 2017
- [6] Parliamentary Monitoring Group. Department of Human Settlements 2016/17 Annual Report, with Auditor-General & DPME input | PMG [Online]. 2017. Available from: <https://pmg.org.za/committee-meeting/25122/> [Accessed: 2019-02-9]
- [7] Klunne WE. Energy efficient housing to benefit South African households. *Boiling Point.* 2002;**48**:27-29
- [8] Overy N. *The Housing Crisis in the Eastern Cape.* Johannesburg: Public Service Accountability Monitor; 2005
- [9] Overen OK, Meyer EL, Makaka G. Thermal, economic and environmental analysis of a low-cost house in Alice, South Africa. *Sustainability.* 2017;**9**:425
- [10] Dear KBG, McMichael AJ. The health impacts of cold homes and fuel poverty. *BMJ.* 2011;**342**:d2807. DOI: 10.1136/bmj.d2807
- [11] Sustainable Energy Africa. *Tackling Urban Energy Poverty in South Africa.* Cape Town: Heinrich Böll Stiftung Southern Africa; 2014
- [12] Eltaweel A, SU Y. Parametric design and daylighting: A literature review. *Renewable and Sustainable Energy Reviews.* 2017;**73**:1086-1103. DOI: 10.1016/j.rser.2017.02.011
- [13] Victoria J, Akhtar S, Akmal W, Wan Z. Bioclimatic design approach in Dayak traditional longhouse. *Procedia Engineering.* 2017;**180**:562-570. DOI: 10.1016/j.proeng.2017.04.215
- [14] Schnieders J, Feist W, Rongen L. Passive Houses for different climate zones. *Energy and Buildings.* 2015;**105**:71-87. DOI: 10.1016/j.enbuild.2015.07.032
- [15] Karava P, Stathopoulos T, Athienitis AK. Airflow assessment in cross-ventilated buildings with operable façade elements. *Building and Environment.* 2011;**46**:266-279. DOI: 10.1016/j.buildenv.2010.07.022
- [16] Overen OK, Meyer EL, Makaka G, Ziuku S, Mamphweli S. Zonal air exchange rate of a passive solar house and resultant sensible air heat transfer. *Indoor and Built Environment.* 2018;**0**:1-13. DOI: 10.1177/1420326X18804605
- [17] Jo JH, Lim JH, Song SY, Yeo MS, Kim KW. Characteristics of pressure distribution and solution to the problems caused by stack effect in high-rise residential buildings. *Building and Environment.* 2007;**42**:263-277. DOI: 10.1016/j.buildenv.2005.07.002

- [18] South African Bureau of Standards. SANS 204: Energy efficiency in buildings; 2011; South Africa. Pretoria: South African Bureau of Standards; 2011. pp. 1-65
- [19] Conradie DCU. South Africa's climatic zones: Today, tomorrow. In: International Green Building Conference and Exhibition. Pretoria: Center of Science and Industrial Research; 2012;2012. pp. 1-9
- [20] South African Bureau of Standards, SANS 10400-XA. The application of National Building Regulations, Part X: Environmental sustainability, Part XA: Energy usage in buildings; 2011; South Africa. Pretoria: South African Bureau of Standards; 2011. pp. 1-17
- [21] Ziuku S, Meyer E. Energy Efficient Building Integrated Photovoltaic Housing. Alice: University of Fort Hare; 2011
- [22] Makaka G, Meyer EL, McPherson M. Thermal behaviour and ventilation efficiency of a low-cost passive solar energy efficient house. *Renewable Energy*. 2008;**33**:1959-1973. DOI: 10.1016/j.renene.2007.11.014
- [23] Moser Y, Gijs MAM. Miniaturized flexible temperature sensor. *Journal of Microelectromechanical Systems*. 2007;**16**:1349-1354
- [24] Rontronic Measurement Solutions. The Capacitive Humidity Sensor—How It Works & Attributes of the Uncertainty Budget. New York: Rontronic Measurement Solutions; 2016
- [25] Campbell Scientific INC. HMP60 Temperature and Relative Humidity Probe. Utah: Campbell Scientific; 2010
- [26] Campbell Scientific INC. Solar Radiation Shields: For Temperature/Relative Humidity Sensors. Utah: Campbell Scientific; 2015
- [27] Ruiz-Arias JA, Gueymard CA. Worldwide inter-comparison of clear-sky solar radiation models: Consensus-based review of direct and global irradiance components simulated at the earth surface. *Solar Energy*. 2018;**168**:10-29
- [28] Gueymard CA. Cloud and albedo enhancement impacts on solar irradiance using high-frequency measurements from thermopile and photodiode radiometers. Part 1 : Impacts on global horizontal irradiance. *Solar Energy*. 2017;**153**:755-765. DOI: 10.1016/j.solener.2017.05.004
- [29] Kipp & Zonen. Instruction manual—Pyranometer and albedometer. Delft: Kipp & Zonen; 2015
- [30] Kerr J, Thurtell G, Tanner C. An integrating pyranometer for climatological observer stations and mesoscale networks. *Journal of Applied Meteorology*. 1967;**6**:688-694. DOI: 10.1175/1520-0450(1967)006<0688:aipfco>2.0.co;2
- [31] Hinrichs R, Kleinbach M. *Energy: Its Use and the Environment*. 5th ed. New York: BROOKS/COLE; 2013
- [32] Paulescu M, Paulescu E, Gravila P, Badescu V. *Weather Modeling and Forecasting of PV Systems Operation*. London: Springer Science & Business Media; 2012
- [33] Marzo A, Trigo M, Alonso-Montesinos J, Martínez-Durbán M, López G, Ferrada P, et al. Daily global solar radiation estimation in desert areas using daily extreme temperatures and extraterrestrial radiation. *Renewable Energy*. 2017;**113**:303-311. DOI: 10.1016/j.renene.2017.01.061
- [34] Overen OK, Meyer EL, Makaka G. Perimeter walls solar heat gain, a mechanism for building design. In: 11 Built Environment Conference; 2017. pp. 680-691

[35] Szokolay SV. Introduction to Architectural Science: The Basis of Sustainable Design. Vol. 8. 2nd ed. Oxford: Elsevier; 2008

[36] Kaşka Ö, Yumrutaş R, Orhan A. Theoretical and experimental investigation of total equivalent temperature difference (TETD) values for building walls and flat roofs in Turkey. *Energy Conversion and Management*. 2008;**50**:2818-2825. DOI: 10.1016/j.enconman.2009.06.027

[37] Kreider JF, Curtiss PS, Rabl A. Heating and Cooling of Buildings: Design for Efficiency. 2nd ed. Denver: CRC Press; 2009

[38] ASHRAE. ASHRAE Handbook: Fundamentals. Am. Soc. Heating, Refrig. Air Cond. Eng. Atlanta, 32, 2005, TC 4.7, Energy Calculations. DOI: 10.1039/c1cs15219j

[39] Robert AP. Cooling load calculation. In: ASHRAE Handbook-Fundamentals, SI. Vol. 2001. New York: ASHRAE; 2001. pp. 1-106

[40] SABS. SANS 204:2011—South African National Standard: Energy efficiency in buildings. Pretoria: South African Bureau of Standards; Vol. 1. 2011